Modeling and Characterization of Frequency-Domain Thermal Impedance for IGBT Module Through Heat Flow Information

Ke Ma, *Senior Member, IEEE*, Mengqi Xu, *Student Member, IEEE*, and Bo Liu

***Abstract*—Frequency-domain modeling is a relatively new approach for thermal impedance description of power semiconductor devices, and it has shown promising advantages to analyze the multitimescale thermal dynamics of power semiconductor devices under complex mission profiles. However, parameters in the frequency-domain thermal model are still difficult to be accurately extracted, and sometimes the extraction process would be complicated and ambiguous depending on the construction of power devices and heat sink. This article proposes a new method to identify these key parameters of the frequency-domain thermal model for power semiconductors. The proposed approach utilizes the information of heat flowing out of device and only requires temperature responses of three different locations in the heat path of insulated-gate bipolar transistor (IGBT) module under a step power-loss. By the proposed approach, the critical frequencies in the frequency-domain thermal model of IGBT module can be extracted more easily and accurately. The effectiveness of the proposed method is also validated by simulations and experiments.**

***Index Terms*—Power electronics, power semiconductor device, thermal network.**

I. Introduction

POWER electronic devices, especially insulated-gate bipolar transistor (IGBT) modules, have been widely used in many important applications such as motor drives, renewable energy generations, transportations, and power transmission. In these applications, there are fast growing requirements for the reliability of converter systems, and the reliability of power electronic devices, including failure mechanisms [1]–[6], stress analysis [7]–[12], lifetime prediction [13]–[18], condition monitoring [19], [20], and thermal control [21], [22] is becoming more important. It has been widely accepted that thermal stress of power electronic devices is one of the major causes of failure [5]. Consequently, the correct estimation for the complex thermal dynamics of power semiconductor devices under certain mission profile is crucial for reliability design.

Foster type and Cauer type *RC* networks are most commonly used models for thermal dynamics description of power semiconductors. However, both of the models have their limitations: for Cauer model, normally it is hard to obtain accurate *RC* parameters because Cauer type *RC* network is built based on heat path through physical structure/materials of the device, and the *RC* parameters have to be determined with the help of finite element method (FEM) simulations and careful calibrations. For Foster model, it has no physical meaning for each of the *RC* parameter, which is determined by mathematical fitting of measured temperatures between two physical points, so only overall temperature behaviors between measured points can be guaranteed. If extend the Foster model with the thermal network outside device, such as the thermal grease and heat sink, Foster model will cause unrealistic estimation of thermal behaviors either inside or outside of the device [23].

In order to improve the prediction accuracy of thermal dynamics of power semiconductor devices, some efforts have been proposed in the last decade. The thermal analysis of power device is separated into multiple modeling levels (short term, medium term, and long term) according to the timescales of the interested thermal dynamics [13]. One of the problems of this approach is that many complex models at different physics domains are involved, and there is lack of connection among models at different timescales. Besides, external cooling conditions need to be carefully considered in certain timescales but the thermal impedance models of device used in this approach are unable to be connected with external thermal network of heat sink, leading to unrealistic thermal dynamics in a wide range of timescales. A 3-D lumped thermal model has been proposed in [24]. This approach selects key points of each layer in IGBT module and creates thermal impedance among the selected points by taking into account thermal coupling and thermal boundary conditions. This 3-D lumped thermal model can estimate detailed and accurate temperatures of the power module in different locations and layers. However, the extraction process of the *RC* element values is complicated, and multiple FEM simulations and calibrations are necessary in order to obtain temperature responses of each layer inside the device. This model is also difficult to be connected with external cooling

---

Manuscript received November 28, 2019; revised May 17, 2020; accepted July 6, 2020. Date of publication July 14, 2020; date of current version September 22, 2020. This work was supported by National Key Research and Development Program of China under Grant 2018YFB0905802. Recommended for publication by Associate Editor H. Wang. *(Corresponding author: Ke Ma.)*

Ke Ma, Mengqi Xu, and Bo Liu are with the Key Laboratory of Control of Power Transmission and Conversion, Ministry of Education, Shanghai Jiao Tong University, Shanghai 200240, China, and also with the Department of Electrical Engineering, Shanghai Jiao Tong University, Shanghai 200240, China (e-mail: kema@sjtu.edu.cn; mengqixu@sjtu.edu.cn; bo_liu@sjtu.edu.cn).

Color versions of one or more of the figures in this article are available online at https://ieeexplore.ieee.org.

Digital Object Identifier 10.1109/TPEL.2020.3009257

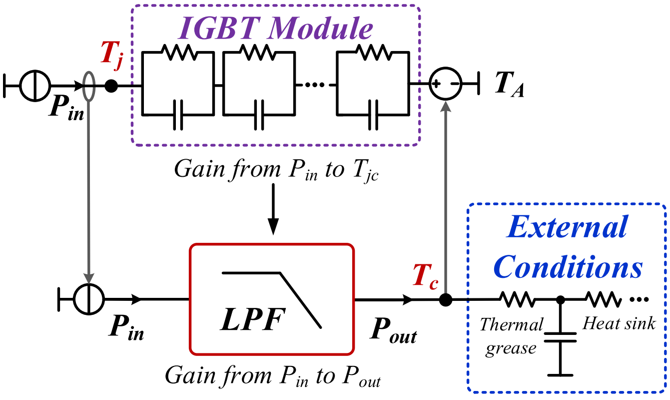

Fig. 1. Frequency-domain thermal model for power semiconductor devices.

conditions because it is supposed that the cooling conditions have to be ideal and fixed during extraction process.

Another approach to handle multitime scale thermal dynamics of power device is based on frequency-domain modeling approach [23]. It has been discovered that the gain of heat flow from P_{in} (injected power-loss/heat into device) to P_{out} (heat flowing out of device) behaves as a low-pass filter (LPF) under frequency domain. A new thermal impedance structure which adds an LPF with an extra thermal path was proposed, as illustrated in Fig. 1. The first thermal path is used for estimating junction temperature inside the power device and is not connected with external thermal networks outside of device. The second thermal path with LPF, which provides correct heat flow behaviors, can be connected with external cooling conditions, and the adding thermal path is used to provide the case temperature for the first path as temperature reference. This model is claimed to achieve a more correct estimation of multitimescale thermal dynamics. Moreover, the parameters of this model can be obtained by observing temperature behaviors of device under certain testing conditions without knowing its internal structure and materials, avoiding potential error introduced by FEM simulation and its boundary conditions. Some applications of this new model have also emerged recently [25]–[29].

Nevertheless, the characterization of the parameters for LPF is a key in the abovementioned frequency-domain thermal model. They can be extracted from Foster-type thermal impedance between junction and case, as stated in [23]. However, the process of this extraction method is complicated and ambiguous, and the accuracy of results cannot be always guaranteed, as explained in the following part of this article. If the parameters of LPF in Fig. 1 are inaccurate, the estimation for case temperature offered by the second thermal path will be different from reality, leading to unrealistic estimation for junction temperature in the first thermal path, so the extraction of LPF is crucial for this thermal modeling method.

In this article, a new approach to model and characterize the LPF of frequency-domain thermal model for power semiconductor device is proposed by utilizing the information of heat flowing out of device and it only requires temperature responses of three different locations in the heat path of IGBT module under a step power-loss. The critical frequencies in the frequency-domain thermal model of IGBT module can be extracted more easily and accurately by using the proposed approach. The effectiveness of the proposed method is also validated by simulations and experiments.

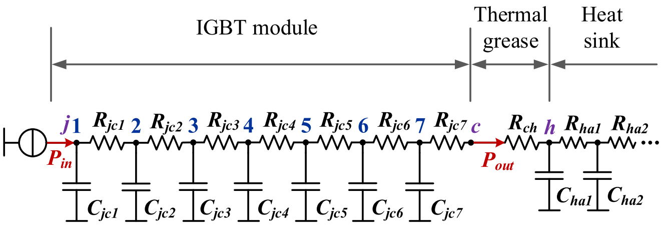

Fig. 2. Seven-layer Cauer thermal network based on Fig. 3 as reference of study.

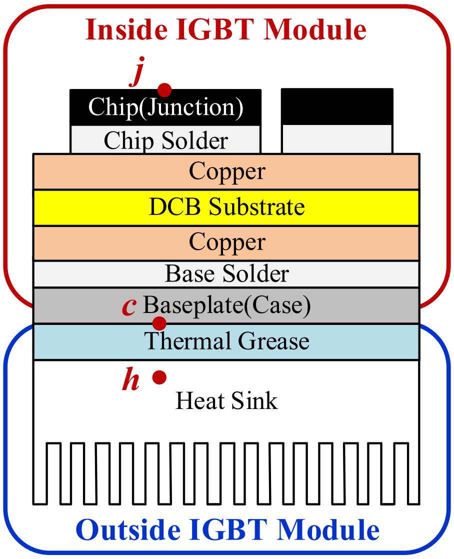

Fig. 3. Construction of an IGBT module as reference for study.

II. Conventional Characterization Method for Critical Frequencies of LPF in Frequency-Domain Thermal Impedance Model

This part introduces the principle of frequency-domain model and the existing method of parameter characterization. Also, the problems of the existing method are analyzed in detail.

A seven-layer Cauer type thermal network for an IGBT module from [23] is applied as benchmark for study, as illustrated in Fig. 2. This Cauer model is extracted based on the heat path and physical structure/material of a 1700 V/100 A IGBT module, as shown in Fig. 3. Thermal parameters of single chip in this IGBT module are listed in Table I. It can be assumed that the network in Fig. 2 and parameters in Table I can correctly reflect the dynamic thermal behaviors of IGBT module under the given conditions [23].

A. Review on the Frequency-Domain Thermal Model

The frequency-domain thermal model is proposed based on the discovery that the heat flow of IGBT behaves like an LPF

TABLE I
THERMAL PARAMETERS FOR THE IGBT MODULE OF Fig. 3

Layers	Thermal Resistance (K/W)		Thermal Capacitance (J/K)	
Chip	R_{jc1}	0.0194	C_{jc1}	0.1021
Chip solder	R_{jc2}	0.0034	C_{jc2}	0.0179
Copper	R_{jc3}	0.0040	C_{jc3}	0.2092
DCB	R_{jc4}	0.1732	C_{jc4}	0.5118
Copper	R_{jc5}	0.0030	C_{jc5}	0.2732
Base solder	R_{jc6}	0.0048	C_{jc6}	0.0517
Baseplate	R_{jc7}	0.0209	C_{jc7}	4.0898
Thermal grease	R_{ch}	0.0518	NA	

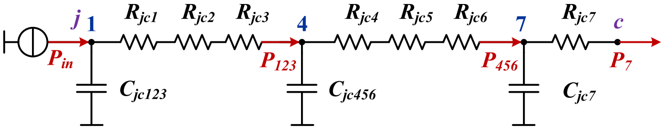

Fig. 4. Transforming of the seven-layer Cauer network to three cascaded LPFs.

under frequency-domain and the detailed derivation is explained as follows.

As stated in [23], the gains of heat flow from input (chip) to each layer of device $G_{P_{\mathrm{in}}P_1}$ to $G_{P_{\mathrm{in}}P_7}$ in the reference Cauer model of Fig. 2 are generally seen as a series of LPFs, which can be classified into three dominant groups ($G_{P_{\mathrm{in}}P_1}$ to $G_{P_{\mathrm{in}}P_3}$, $G_{P_{\mathrm{in}}P_4}$ to $G_{P_{\mathrm{in}}P_6}$, and $G_{P_{\mathrm{in}}P_7}$). The frequency behaviors of these heat gains in each group are very similar to each other, so the reference seven-layer Cauer thermal model can be degraded to three cascaded LPFs at first-order, where C_{jc123}, C_{jc456}, C_{jc7} represent the virtual thermal capacitances for each dominant group of layers, and P_{123}, P_{456}, P_7 represent the virtual heat flowing out of each dominant group of layers, as shown in Fig. 4.

Therefore, the transfer function for the heat or power loss from input to output of Fig. 2 $G_{P_{\mathrm{in}}P_{\mathrm{out}}}$ (s) can be estimated as the heat gain G_{LPF} (s) of Fig. 4

$$\begin{aligned} G_{P_{\mathrm{in}}P_{\mathrm{out}}}(s) &\approx G_{\mathrm{LPF}}(s) \\ &= \frac{2\pi f_{\mathrm{cr1}}}{s+2\pi f_{\mathrm{cr1}}} \cdot \frac{2\pi f_{\mathrm{cr2}}}{s+2\pi f_{\mathrm{cr2}}} \cdot \frac{2\pi f_{\mathrm{cr3}}}{s+2\pi f_{\mathrm{cr3}}} \end{aligned} \tag{1}$$

where f_{cr1}, f_{cr2}, f_{cr3} are the critical frequencies of each layer in Fig. 4. As a result, a frequency-domain thermal model has been thereby proposed according to this discovery, as illustrated in Fig. 1. Compared with Foster thermal network, it only adds another thermal path to describe the heat flow behavior. This thermal path with an LPF is directly connected with external cooling conditions and provides the first thermal path with case temperature.

B. Problems of Existing Characterization Method for the Critical Frequencies Through $Z_{P_{\mathrm{in}}T_{\mathrm{jc}}}$

The accuracy of parameters should be ensured before applying frequency-domain model in practice. The existing method of parameter extraction is based on the transfer function of thermal impedance between junction and case $Z_{P_{\mathrm{in}}T_{\mathrm{jc}}}$ (s) because it discovers that $Z_{P_{\mathrm{in}}T_{\mathrm{jc}}}$ is closely related to LPF in the second thermal path.

The thermal impedance between junction and case $Z_{P_{\mathrm{in}}T_{\mathrm{jc}}}$ (s) of Fig. 4 can be represented as

$$\begin{aligned} Z_{P_{\mathrm{in}}T_{\mathrm{jc}}}(s) &= Z_{P_{\mathrm{in}}T_{j4}}(s) + Z_{P_{\mathrm{in}}T_{47}}(s) + Z_{P_{\mathrm{in}}T_{7c}}(s) \\ &= \frac{P_{123}(s)}{P_{\mathrm{in}}(s)} \cdot \frac{T_j(s)-T_4(s)}{P_{123}(s)} + \frac{P_{456}(s)}{P_{\mathrm{in}}(s)} \\ &\quad \cdot \frac{T_4(s)-T_7(s)}{P_{456}(s)} + \frac{P_7(s)}{P_{\mathrm{in}}(s)} \cdot \frac{T_7(s)-T_c(s)}{P_7(s)} \\ &= G_{P_{\mathrm{in}}P_{123}}(s) \cdot \sum_{i=1}^{3} R_{\mathrm{jc}i} + G_{P_{\mathrm{in}}P_{456}}(s) \\ &\quad \cdot \sum_{i=4}^{6} R_{\mathrm{jc}i} + G_{P_{\mathrm{in}}P_7}(s) \cdot R_7. \end{aligned} \tag{2}$$

As the accuracy of thermal prediction is mainly dependent on low-frequency band, which will be explained in the following part in detail, (2) can be simplified as (3) by ignoring some of the high-frequency band behaviors in the $G_{P_{\mathrm{in}}P_{456}}$ and $G_{P_{\mathrm{in}}P_7}$

$$\begin{aligned} Z_{P_{\mathrm{in}}T_{\mathrm{jc}}}(s) &\approx G_{P_{\mathrm{in}}P_{123}}(s) \cdot \sum_{i=1}^{3} R_{\mathrm{jc}i} + G_{P_{123}P_{456}}(s) \\ &\quad \cdot \sum_{i=4}^{6} R_{\mathrm{jc}i} + G_{P_{456}P_7}(s) \cdot R_7 \\ &= \frac{\sum_{i=1}^{3} R_{\mathrm{jc}i}}{1+s\cdot\frac{1}{2\pi f_{\mathrm{cr1}}}} + \frac{\sum_{i=4}^{6} R_{\mathrm{jc}i}}{1+s\cdot\frac{1}{2\pi f_{\mathrm{cr2}}}} + \frac{R_7}{1+s\cdot\frac{1}{2\pi f_{\mathrm{cr3}}}}. \end{aligned} \tag{3}$$

It can be seen that (3) is equivalent to the form of a three-layer Foster thermal network under frequency domain, and the critical frequencies f_{cr1} to f_{cr3} in the Foster model are the same as the three cascaded LPFs. Therefore, the thermal impedance $Z_{P_{\mathrm{in}}T_{\mathrm{jc}}}$ contains all the information of the critical frequencies in the LPFs, so it is possible to extract these frequencies through $Z_{P_{\mathrm{in}}T_{\mathrm{jc}}}$. The process of extraction in [23] is generally reviewed and stated as follows.

The first step is to fit $Z_{P_{\mathrm{in}}T_{\mathrm{jc}}}$ (t) in the time domain by a multi-layers Foster model, which can be transferred into frequency domain form as $Z_{P_{\mathrm{in}}T_{\mathrm{jc}}}$ (s). Then, by applying a deviating operator $F(x)$ to the $Z_{P_{\mathrm{in}}T_{\mathrm{jc}}}$ (s), the slope deviation on the amplitude of $Z_{P_{\mathrm{in}}T_{\mathrm{jc}}}$ (s) can be identified

$$F(x) = \frac{d^2}{dx^2} 20 \times \log_{10}(|Z_{P_{\mathrm{in}}T_{\mathrm{jc}}}(x)|) \tag{4}$$

where $Z_{P_{\mathrm{in}}T_{\mathrm{jc}}}$ (s) is converted to the function of f as $Z_{P_{\mathrm{in}}T_{\mathrm{jc}}}$ (f) by replacing s with $2\pi f \cdot j$, and then $Z_{P_{\mathrm{in}}T_{\mathrm{jc}}}$ (f) is converted into the function of x as $Z_{P_{\mathrm{in}}T_{\mathrm{jc}}}$ (x) by replacing f with 10^x.

As is shown in Fig. 5, there are three minimum turning points in $F(x)$ and the critical frequencies can be solved by setting zero to the derivative of $F(x)$. In this case, three frequencies can be solved out with ascending order: $f_1 = 0.297$, $f_2 = 1.422$, and $f_3 = 74.129$ Hz, which are closely related to critical frequencies in the heat-gains but are still slightly different. The main reason

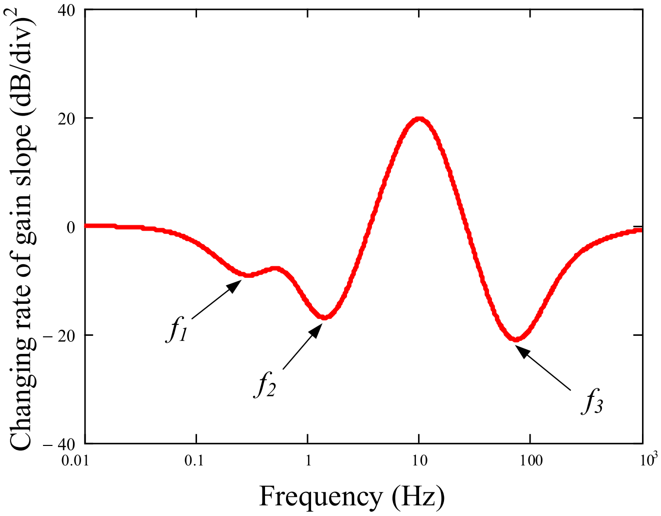

Fig. 5. Slope deviation on the amplitude of $Z_{P_{\mathrm{in}}T_{\mathrm{jc}}}$ (s) and identified critical frequencies.

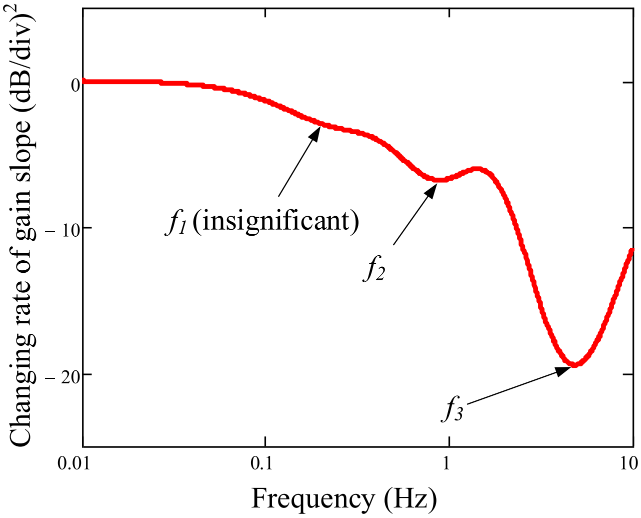

Fig. 6. Slope deviation on the amplitude of $Z_{P_{\mathrm{in}}T_{\mathrm{jc}}}(s)$ with insignificant critical frequencies.

is that the critical frequencies in the heat-gains are the three representative frequencies in the three dominant groups ($G_{P_{\mathrm{in}}P_1}$ to $G_{P_{\mathrm{in}}P_3}$, $G_{P_{\mathrm{in}}P_4}$ to $G_{P_{\mathrm{in}}P_6}$, and $G_{P_{\mathrm{in}}P_7}$). It can been seen from (3) that simplifications are required in order to build a relationship between $Z_{P_{\mathrm{in}}T_{\mathrm{jc}}}$ (s) and G_{LPF} (s). Therefore, the frequencies f_1–f_3 transferred from the turning points in the plot of $F(x)$ cannot be seen as the critical frequencies in LPF. As stated in [23], one of the solutions is to refit $Z_{P_{\mathrm{in}}T_{\mathrm{jc}}}$ (t) in time domain with new boundary conditions based on f_1–f_3 and then three new frequencies of $f_{cr1} = 0.38$, $f_{cr2} = 1.36$, and $f_{cr3} = 70.36$ Hz can be resolved. f_{cr1}–f_{cr3} have been validated in [23] and will be seen as reference frequencies in this article.

However, there are several problems during the process of extracting critical frequencies from $Z_{P_{\mathrm{in}}T_{\mathrm{jc}}}$. For example, the initial fitting of time-domain thermal impedance $Z_{P_{\mathrm{in}}T_{\mathrm{jc}}}$ (t) by a multilayered Foster model is necessary because frequency-domain form of $Z_{P_{\mathrm{in}}T_{\mathrm{jc}}}$ (s) is obtained by Laplace transform from Foster type $Z_{P_{\mathrm{in}}T_{\mathrm{jc}}}$ (t). Therefore, $Z_{P_{\mathrm{in}}T_{\mathrm{jc}}}$ (s) is slightly different from original thermal impedance $Z_{P_{\mathrm{in}}T_{\mathrm{jc}}}$ and the critical frequencies extracted from $Z_{P_{\mathrm{in}}T_{\mathrm{jc}}}$ (s) are also different from reality, leading to requirement of refitting time-domain thermal impedance in multiple times.

Another problem is that if one of the turning points is insignificant, the fitting process would be more complicated. An example has been plotted in Fig. 6, it can be seen that the frequency f_1 is hard to identify because the derivative is not equal to zero at this point. This problem is mentioned in [23] and one possible solution is given that the influence of other frequencies should be removed first before identifying the insignificant points.

Moreover, it is difficult to set the boundary conditions of fitting algorithm for $Z_{P_{\mathrm{in}}T_{\mathrm{jc}}}$ (t) because the accuracy of each frequency identified from $F(x)$ is unknown. As mentioned above, three initially identified frequencies are $f_1 = 0.297$, $f_2 = 1.422$, and $f_3 = 74.129$ Hz, the errors compared with the reference ones at $f_{cr1} = 0.38$, $f_{cr2} = 1.36$, and $f_{cr3} = 70.36$ Hz are -21.84%, 4.56%, and 5.36%, respectively. The large error of the lowest frequency f_1 brings difficulty to delimit the boundary conditions for fitting $Z_{P_{\mathrm{in}}T_{\mathrm{jc}}}$ (t). As a matter of fact, the dynamic performance of thermal behavior is highly related to the accuracy of lowest frequency f_1, as shown in Fig. 7, compared with reference seven-layer Cauer thermal network, the case temperatures are predicted in three conditions where different critical frequencies have the same error of 30% are applied. First, the condition that f_x is 30% larger than $f_{\mathrm{cr}x}$ is considered and the corresponding frequencies are as follows:

1) $f_1 = 0.494, f_2 = 1.36$, and $f_3 = 70.36$ Hz;
2) $f_1 = 0.38, f_2 = 1.768$, and $f_3 = 70.36$ Hz;
3) $f_1 = 0.38, f_2 = 1.36$ and $f_3 = 91.468$ Hz.

Then, the condition that f_x is 30% smaller than $f_{\mathrm{cr}x}$ is considered and the corresponding frequencies are as follows:

1) $f_1 = 0.266, f_2 = 1.36$, and $f_3 = 70.36$ Hz;
2) $f_1 = 0.38, f_2 = 0.952$, and $f_3 = 70.36$ Hz;
3) $f_1 = 0.38, f_2 = 1.36$, and $f_3 = 49.25$ Hz.

It can be concluded from Fig. 7 that unrealistic estimation for thermal behaviors will be experienced if the lowest frequency f_1 is inaccurately extracted. Thus, the accuracy of the lowest frequency in the G_{LPF} should be ensured. However, it is difficult to ensure the accuracy of f_1 in the existing method of extracting frequencies through $Z_{P_{\mathrm{in}}T_{\mathrm{jc}}}$ because each frequency during curve fitting is given equal weight in the expression of the Foster network, as can be seen in (3).

III. CRITICAL FREQUENCIES EXTRACTION BY UTILIZING HEAT FLOW INFORMATION

A. Modeling and Analysis of the Critical Frequencies Information Contained in Heat Flow

Due to the complexity of extracting critical frequencies from $Z_{P_{\mathrm{in}}T_{\mathrm{jc}}}$, other transfer functions related to the critical frequencies can be considered. As mentioned in Section II, $G_{P_{\mathrm{in}}P_{\mathrm{out}}}$ (transfer function of gain from input power-loss P_{in} to heat flowing out of device P_{out}) can be seen as three cascaded LPFs,

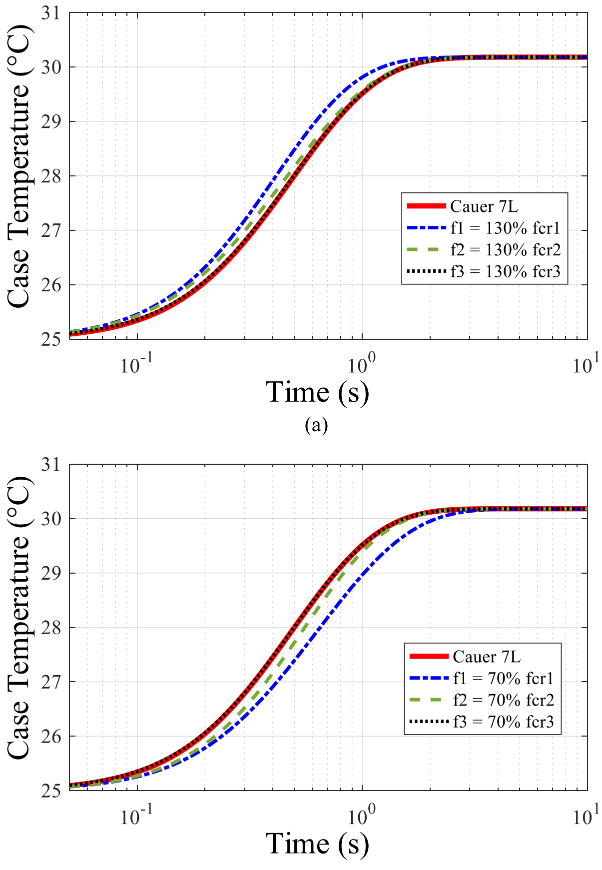

(a)

(b)

Fig. 7. Comparison of estimated case temperatures with 30% error of different critical frequencies. (a) f_x is 30% larger than $f_{\mathrm{cr}x}$. (b) f_x is 30% smaller than $f_{\mathrm{cr}x}$.

so $G_{P_{\mathrm{in}}P_{\mathrm{out}}}$ is another potential transfer function to identify the critical frequencies in the LPF of second heat path in Fig. 1. Compared with $Z_{P_{\mathrm{in}}T_{\mathrm{jc}}}$, $G_{P_{\mathrm{in}}P_{\mathrm{out}}}$ has more advantages since it is purely composed of critical frequencies as represented in (1) and $Z_{P_{\mathrm{in}}T_{\mathrm{jc}}}$ is not only related to critical frequencies but also related to the thermal resistances as represented in (3), adding uncertainties during the process of parameter extraction. Consequently, it is more promising to extract the critical frequencies through $G_{P_{\mathrm{in}}P_{\mathrm{out}}}$ for LPF in the frequency-domain thermal model.

As for the input of $G_{P_{\mathrm{in}}P_{\mathrm{out}}}$, P_{in} is the heat source/power loss generated on the chip and is defined as a step signal in the time domain, the frequency domain expression of P_{in} can be represented as

$$P_{\mathrm{in}}(s) = \frac{P_{\mathrm{in}}}{s} \tag{5}$$

where s is the Laplace operator and P_{in} is a constant.

As mentioned above, the reference seven-layer Cauer thermal model can be simplified as three cascaded LPFs at first-order according to the behaviors of heat gains. By combining (1) and (5), $P_{\mathrm{out}}(s)$ can be calculated as

$$P_{\mathrm{out}}(s) = P_{\mathrm{in}}(s)\cdot G_{P_{\mathrm{in}}P_{\mathrm{out}}}(s)$$

$$\begin{aligned}
&= \frac{P_{\mathrm{in}}}{s}\cdot\frac{2\pi f_{\mathrm{cr}1}}{s+2\pi f_{\mathrm{cr}1}}\cdot\frac{2\pi f_{\mathrm{cr}2}}{s+2\pi f_{\mathrm{cr}2}}\cdot\frac{2\pi f_{\mathrm{cr}3}}{s+2\pi f_{\mathrm{cr}3}}\\
&= \frac{P_{\mathrm{in}}}{s} - \frac{f_{\mathrm{cr}2}f_{\mathrm{cr}3}}{(f_{\mathrm{cr}2}-f_{\mathrm{cr}1})(f_{\mathrm{cr}3}-f_{\mathrm{cr}1})}\cdot\frac{P_{\mathrm{in}}}{s+2\pi f_{\mathrm{cr}1}}\\
&\quad - \frac{f_{\mathrm{cr}1}f_{\mathrm{cr}3}}{(f_{\mathrm{cr}1}-f_{\mathrm{cr}2})(f_{\mathrm{cr}3}-f_{\mathrm{cr}2})}\cdot\frac{P_{\mathrm{in}}}{s+2\pi f_{\mathrm{cr}2}}\\
&\quad - \frac{f_{\mathrm{cr}1}f_{\mathrm{cr}2}}{(f_{\mathrm{cr}1}-f_{\mathrm{cr}3})(f_{\mathrm{cr}2}-f_{\mathrm{cr}3})}\cdot\frac{P_{\mathrm{in}}}{s+2\pi f_{\mathrm{cr}3}}.
\end{aligned} \tag{6}$$

By applying inverse Laplace transform to (6), $P_{\mathrm{out}}(t)$ under time domain can be represented as

$$\begin{aligned}
P_{\mathrm{out}}(t) = P_{\mathrm{in}}\Bigg[\varepsilon(t) &- \frac{f_{\mathrm{cr}2}f_{\mathrm{cr}3}}{(f_{\mathrm{cr}2}-f_{\mathrm{cr}1})(f_{\mathrm{cr}3}-f_{\mathrm{cr}1})}\cdot e^{-2\pi f_{\mathrm{cr}1}t}\\
&- \frac{f_{\mathrm{cr}1}f_{\mathrm{cr}3}}{(f_{\mathrm{cr}1}-f_{\mathrm{cr}2})(f_{\mathrm{cr}3}-f_{\mathrm{cr}2})}\cdot e^{-2\pi f_{\mathrm{cr}2}t}\\
&- \frac{f_{\mathrm{cr}1}f_{\mathrm{cr}2}}{(f_{\mathrm{cr}1}-f_{\mathrm{cr}3})(f_{\mathrm{cr}2}-f_{\mathrm{cr}3})}\cdot e^{-2\pi f_{\mathrm{cr}3}t}\Bigg]
\end{aligned} \tag{7}$$

where $\varepsilon(t)$ is a step function in time domain.

It is noted that, the number of critical frequencies identified can be different depending on the selected power modules, set n as the number of critical frequencies, $P_{\mathrm{out}}(s)$ can be represented in a more general form as

$$P_{\mathrm{out}}(s) = \begin{cases} \dfrac{P_{\mathrm{in}}}{s} - \dfrac{P_{\mathrm{in}}}{s+2\pi f_{\mathrm{cr}n}}, n = 1\\[2ex] \dfrac{P_{\mathrm{in}}}{s} - \displaystyle\sum_{i=1}^{n}\left[\frac{\prod_{j\neq i}^{n} f_{\mathrm{cr}j}}{\prod_{j\neq i}^{n}(f_{\mathrm{cr}j}-f_{\mathrm{cr}i})}\cdot\frac{P_{\mathrm{in}}}{s+2\pi f_{\mathrm{cr}i}}\right], n \neq 1 \end{cases} \tag{8}$$

and $P_{\mathrm{out}}(t)$ can be represented as

$$P_{\mathrm{out}}(t) = \begin{cases} P_{\mathrm{in}}\left[\varepsilon(t) - e^{-2\pi f_{\mathrm{cr}n}t}\right], n = 1\\[2ex] P_{\mathrm{in}}\left\{\varepsilon(t) - \displaystyle\sum_{i=1}^{n}\left[\frac{\prod_{j\neq i}^{n} f_{\mathrm{cr}j}}{\prod_{j\neq i}^{n}(f_{\mathrm{cr}j}-f_{\mathrm{cr}i})}\cdot e^{-2\pi f_{\mathrm{cr}i}t}\right]\right\}, n \neq 1 \end{cases} \tag{9}$$

where $\varepsilon(t)$ is a step function in time domain.

The number of critical frequencies for an arbitrary power device can be determined by counting the turning points of the plot of $F(x)$, as shown in Fig. 5. Under most circumstances, the number of critical frequencies is 3 but it can be reduced to 2 limited by the bandwidth of measurement. In this case, the accuracy of higher frequency among the two remaining critical frequencies will be influenced. Fortunately, the error of high-frequency band in LPF seems less important than low-frequency band, as shown in Fig. 7.

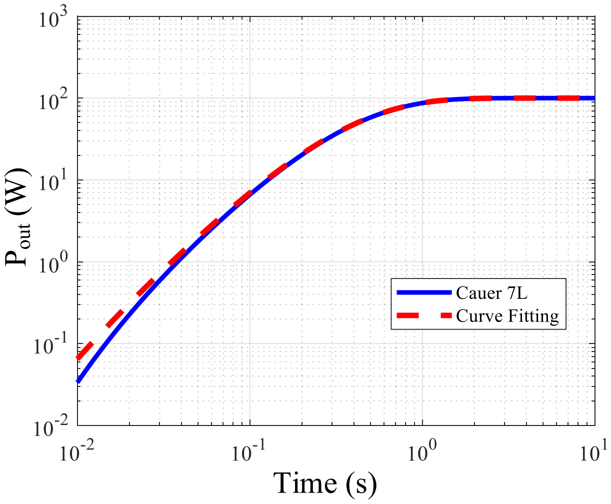

Fig. 8. Simulated and fitted heat flow out of IGBT module.

B. Proposed Extraction Process for the Critical Frequencies and Simulated Validation

A new extraction method is thereby proposed and the basic idea is to extract critical frequencies of LPF by mathematical fitting from $P_{\rm out}\,(t)$ curve. This idea will be verified by simulation first as stated as follows.

The reference seven-layer Cauer thermal network of Fig. 2 is built in PLECS simulation with a step power-loss $P_{\rm in}$ of 100 W at the time of 0 s. Then, record the simulated curve $P_{\rm out}\,(t)$ by using the built-in "Heat Flow Meter" inserted in the thermal path and the recorded data should be imported into MATLAB for curve fitting. The "curve fitting tool" of MATLAB is used in this article during the curve fitting and some processes are necessary before fitting the $P_{\rm out}\,(t)$. First, the recorded data should be plotted in the double logarithm coordinate to demonstrate the information of the whole frequency band and then the customized fitting function (7) should also be changed into the respective form. Second, as mentioned in Section II, it is important to ensure the accuracy of low-frequency band behaviors (0.1–1 Hz in most cases) in LPF during parameter extraction, data before 0.01 s can be excluded during the fitting of $P_{\rm out}\,(t)$ and it turns out that it greatly improves the accuracy of low frequencies by excluding some high-frequency behaviors. Finally, the trust-region algorithm is applied to fit the simulated $P_{\rm out}\,(t)$ curve and three fitted frequencies for $P_{\rm out}\,(t)$ are identified as $f_1 = 0.3802$, $f_2 = 1.363$, and $f_3 = 31.44$ Hz. The fitted curve is shown in Fig. 8. Take the validated critical frequencies of given IGBT module $f_{cr1} = 0.38$, $f_{cr2} = 1.36$, and $f_{cr3} = 70.36$ Hz from [23] as reference, the errors of f_1, f_2, f_3 are 0.05%, 0.22%, and −55.32%, respectively, as shown in Table II.

The major cause of large error in f_3 is that the three cascaded first-order LPFs is a simplified representation for the heat gains, where some high-frequency band behaviors are ignored, leading to the difficulty to ensure the accuracy of identifying highest frequency f_3. Nevertheless, the accuracy of highest frequency f_3 is not as important as the accuracy of others, as shown in Fig. 7. Moreover, the influence of f_{cr3}/f_3-related term is minor in shaping the $P_{\rm out}$ curve by using (7), which means the weight or priority of the term related to f_3 in the curve fitting is much lower than others. Thus, the goodness of fitting is mainly determined by the accuracy of low frequencies, as can be verified in Fig. 8, which has a good agreement with the reference Cauer model after 0.1 s.

TABLE II
COMPARISON OF FREQUENCIES

$f_{cr1\text{-}3}$ (Hz)	$f_{1\text{-}3}$ (Hz)	Error	$f_{1\text{-}3}$' (Hz)	Error
0.38	0.3802	0.05%	0.3802	0.05%
1.36	1.363	0.22%	1.363	0.22%
70.36	31.44	-55.32%	70.57	0.30%

f_{cr1-3} - reference critical frequencies.
f_{1-3} - extracted critical frequencies after fitting $P_{\rm out}\,(t)$.
f_{1-3}' - extracted critical frequencies after fitting $Z_{P_{\rm in}T_{\rm jc}}(t)$.

As a conclusion, the advantage of the proposed method is that it guarantees the accuracy of low-frequency band, but it is hard to ensure the accuracy of highest critical frequency only with the information of $P_{\rm out}$, especially when the highest critical frequency is much higher than the others. In the study case, the reference highest frequency $f_{cr3} = 70.36$ Hz is nearly 52 times of the lower frequency $f_{cr2} = 1.36$ Hz.

As mentioned in Section II, $Z_{P_{\rm in}T_{\rm jc}}$ also contains all the information of critical frequencies, and different from $G_{P_{\rm in}P_{\rm out}}$, the accuracy of the highest critical frequency f_{cr3} in $Z_{P_{\rm in}T_{\rm jc}}$ can be well assured. Therefore, in order to ensure the accuracy of all the identified critical frequencies, it makes sense to utilize both the information of $G_{P_{\rm in}P_{\rm out}}$ and $Z_{P_{\rm in}T_{\rm jc}}$. One solution is to fit $Z_{P_{\rm in}T_{\rm jc}}\,(t)$ with a Foster network, by setting the boundary conditions of fitting algorithm with the ranges of f_1–f_3 generated from $P_{\rm out}$ fitting. According to the definition of thermal impedance [30]–[32], $Z_{P_{\rm in}T_{\rm jc}}(t)$ is calculated by

$$Z_{P_{\rm in}T_{\rm jc}}(t) = \frac{T_j(t) - T_c(t)}{P_{\rm in}}. \tag{10}$$

The errors of f_1–f_3 generated by fitting $P_{\rm out}$ curve are 0.05%, 0.22%, and −55.32%, respectively, so the fitting range for $Z_{P_{\rm in}T_{\rm jc}}\,(t)$ curve can be set as ±0.2%, ±1%, and ±200% around of f_1–f_3 (corresponding to three frequency bands of 0.3794 to 0.3810 Hz, 1.3464 to 1.3736 Hz, and 1.3736 to 93.66 Hz). Under the given fitting conditions, the fitted thermal impedance curve is plotted in Fig. 9. The new critical frequencies obtained by using this proposed method are f_1' = 0.3802, f_2' = 1.363, and f_3' = 70.57 Hz and it turns out that the accuracy of identified highest frequency has been greatly improved. As compared in Table II, the error of each identified frequency is less than 0.5%.

By using the extracted parameters, the estimated thermal dynamics under the given step power loss including junction temperature and heat flow are shown in Fig. 10, which have a good agreement with the reference Cauer model. The procedure of the proposed method to extract parameters of the frequency-domain model is demonstrated as a flow chart in Fig. 11.

The temperature responses of junction (T_j), case (T_c), heatsink (T_h) as well as the input step power loss $(P_{\rm in})$ are

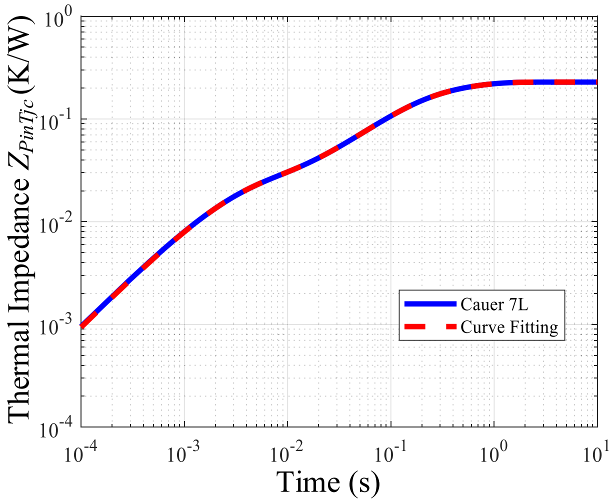

Fig. 9. Simulated and fitted thermal impedance of IGBT module.

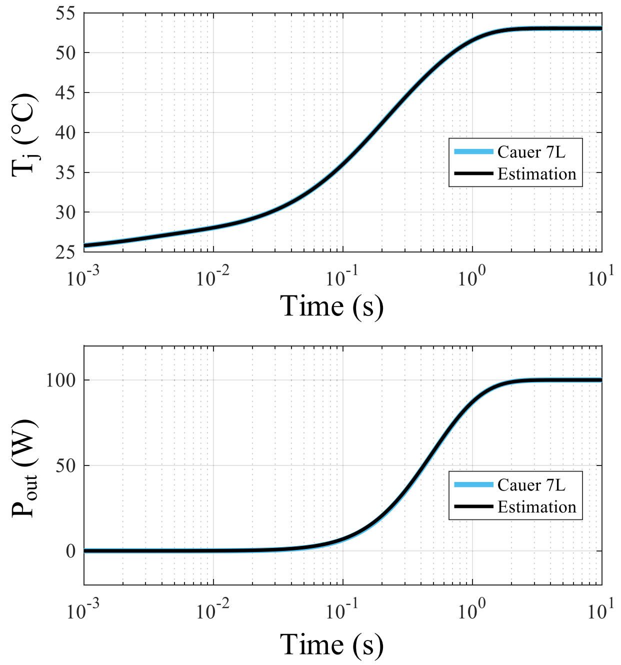

Fig. 10. Comparison of thermal dynamics under a step power loss of 100 W.

recorded, in order to calculate the heat flow $P_{\text{out}}\,(t)$ and thermal impedance $Z_{P_{\text{in}}T_{\text{jc}}}\,(t)$ curve.

Step 1: The first step is to determine the number of frequency n in LPF. The thermal impedance in time-domain $Z_{P_{\text{in}}T_{\text{jc}}}\,(t)$ should be transferred into frequency-domain $Z_{P_{\text{in}}T_{\text{jc}}}\,(s)$ and a deviating operator $F(x)$ is applied to $Z_{P_{\text{in}}T_{\text{jc}}}\,(s)$. In the plot of $F(x)$, the number of turning points n represents there are n critical frequencies in LPF.

Step 2: Equation (9) is used to fit $P_{\text{out}}\,(t)$ curve and n critical frequencies can be initially identified.

Step 3: In order to improve the accuracy of high-frequency band, fit $Z_{P_{\text{in}}T_{\text{jc}}}\,(t)$ curve with an n-layer Foster network, by setting fitting ranges/boundaries of frequencies based on the initially identified frequencies from step 2, respectively.

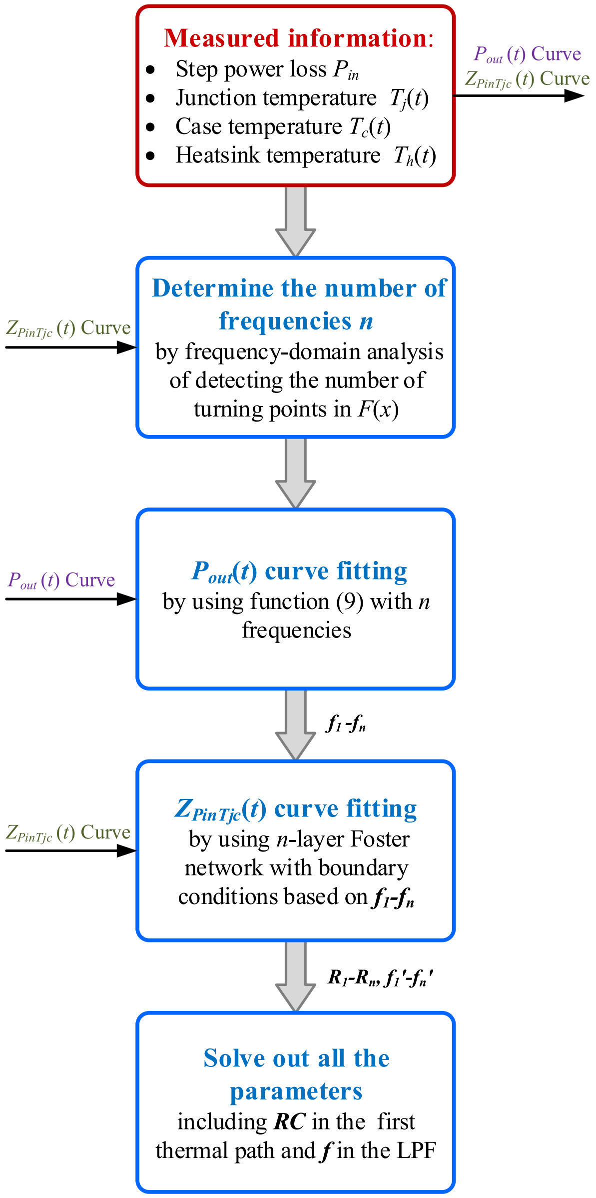

Fig. 11. Flowchart to extract key parameters of the frequency-domain model.

Step 4: Solve out all the parameters in the frequency-domain model, including a Foster network and an LPF.

It is also worth mentioning that the number of critical frequencies is 3 under most circumstances. Therefore, the steps of determining the number of critical frequencies in step 1 can be omitted, in which case all of the parameters in the frequency domain thermal model are extracted by using time-domain recorded curves, thus complicated transformation between time domain and frequency domain can be avoided. Furthermore, $P_{\text{out}}\,(t)$ can be estimated by using temperature responses of case $T_c\,(t)$ and heatsink $T_h\,(t)$ in most cases, which will be explained in Section IV. But heatsink $T_h\,(t)$ is unnecessary if there are measuring instruments to directly measure heat flow.

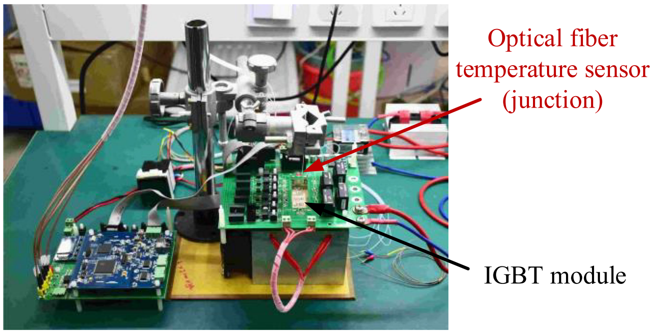

(a)

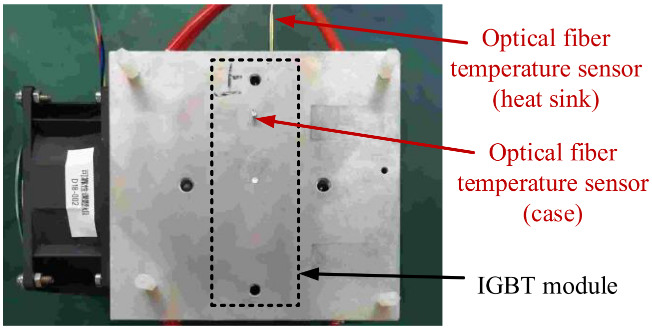

(b)

Fig. 12. Experimental setup and sensor locations. (a) Sensor for junction measurement. (b) Sensors for case and heat sink measurement.

IV. EXPERIMENTAL VALIDATION

A. *Experimental Setup and Measurements Implementations*

A 650 V/75 A IGBT power module is used to validate the proposed method in this article. Three optical fiber temperature sensors are set to junction, case and heatsink for thermal measurement, as shown in Fig. 12. The measuring point for the junction node is in the center of an IGBT chip, and the measuring points for the case node and the heat sink node are set very close to each other because it is difficult to measure heat flow directly. In this article, (11) is used to estimate the P_{out} (heat flowing out of IGBT module). The small distance between case and heat sink measuring points has to be assured in order to avoid thermal capacitance measured in the thermal grease layer, which is considered as pure thermal resistance R_{ch} in most cases

$$P_{\mathrm{out}}(t)=\frac{T_c(t)-T_h(t)}{R_{\mathrm{ch}}}. \tag{11}$$

As can be seen from (11), R_{ch} is a constant and the dynamics of P_{out} should not be affected by the errors of R_{ch}, and only the temperature measurements of case and heatsink are needed. All of the sensors are ensured to be allied in the same heat path of one IGBT chip, which are widely adopted by device manufacturers and they are consistent with the standards for thermal characterizations of power semiconductors, such as MIL-STD-883G [33], JESD51-4A [34] standards. The sensors applied in the setup have a measurement range of -40 °C to $+250$ °C with an accuracy of ± 0.3 to 0.8 °C, the response time is limited to 5 ms.

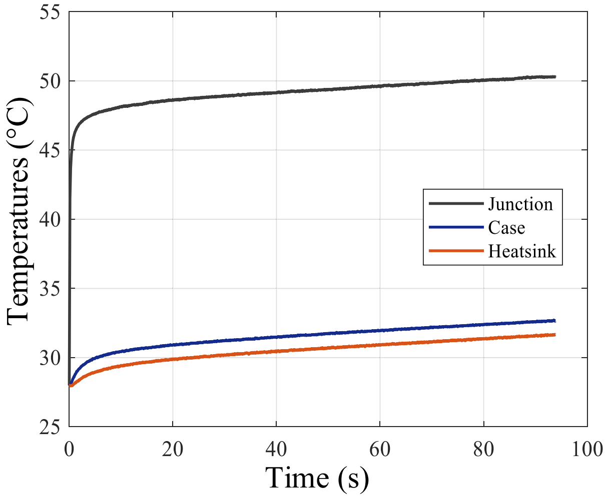

Fig. 13. Experimental temperature responses of three locations under a step power-loss of 33.4 W into an IGBT module.

B. *Experimental Results Using Proposed Method*

According to the flow chart of extracting parameters in Fig. 11, the first step is to record three temperature responses of device under a step power loss. The temperature curves of junction, case and heat sink are measured during turn-OFF process with constant current of 25.3 A and conduction voltage of 1.32 V, which is equivalent to a step power-loss of 33.4 W applied to the thermal networks of the power module, as shown in Fig. 13. The reason for measuring during turn-OFF process is that the conduction voltage of device is not constant during turn-ON process, so the injected power-loss cannot be seen as a step signal.

After acquiring the temperature responses of junction, case and heatsink, thermal impedance $Z_{P_{\mathrm{in}}T_{\mathrm{jc}}}(t)$, and heat flow $P_{\mathrm{out}}(t)$ can be calculated by (10) and (11), respectively. The number of critical frequencies for this power module is 3, which is determined by identifying the number of turning points in the plot of $F(x)$. According to the flow shown in Fig. 11, the next step is to fit $P_{\mathrm{out}}(t)$ curve. By fitting $P_{\mathrm{out}}(t)$ curve using customized function (7) in MATLAB, three frequencies $f_1 = 0.1379$, $f_2 = 1.428$, and $f_3 = 4.556$ Hz can be identified. It is noticed that data of $P_{\mathrm{out}}(t)$ before 0.1 s should be ignored when curve fitting due to the accuracy limitation of sensors, as shown in Fig. 14(a). Therefore, the fitted result of highest frequency f_3 is also inaccurate because 0.1 s corresponds to a cut-off frequency around 1.5 Hz. One solution to this problem is to improve the level of input power-loss P_{in}, leading to the improvement of the steady-state value of $P_{\mathrm{out}}(t)$ without changing its dynamic performance.

The next step of extraction is to fit $Z_{P_{\mathrm{in}}T_{\mathrm{jc}}}(t)$ curve and the fitting range of frequencies is set the same as Section II, that is, $\pm 0.2\%$, $\pm 1\%$, and $\pm 200\%$. As the response time of sensors is limited to 5 ms, corresponding to a cut-off frequency around 30 Hz, data of $Z_{P_{\mathrm{in}}T_{\mathrm{jc}}}(t)$ curve before 0.01 s in Fig. 14(b) are ignored when curve fitting and the fitted curve has a good agreement with experiment result after 0.02 s. The final identified

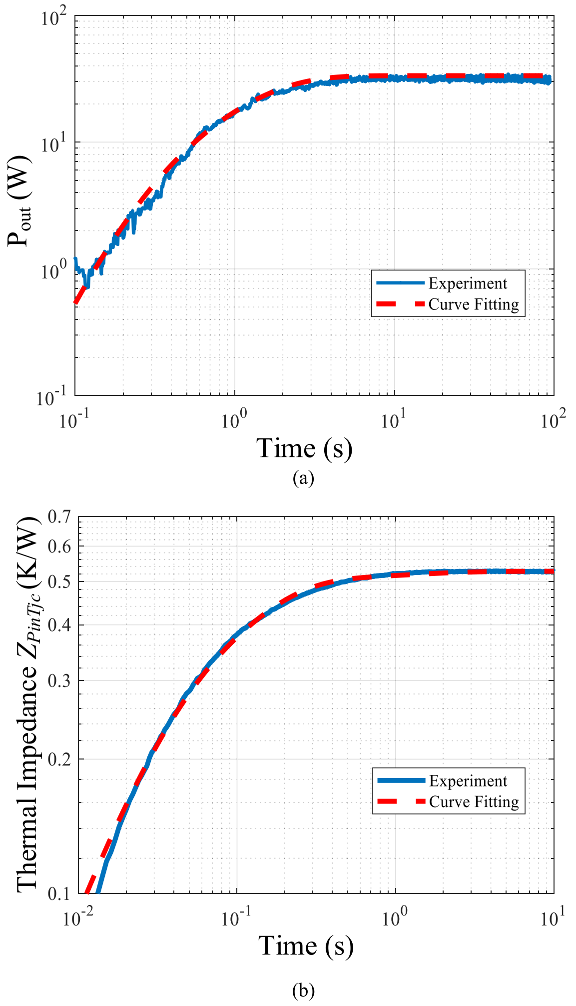

(a)

(b)

Fig. 14. Critical experimental curves and respective fitted curves. (a) Heat flow. (b) Thermal impedance of junction to case.

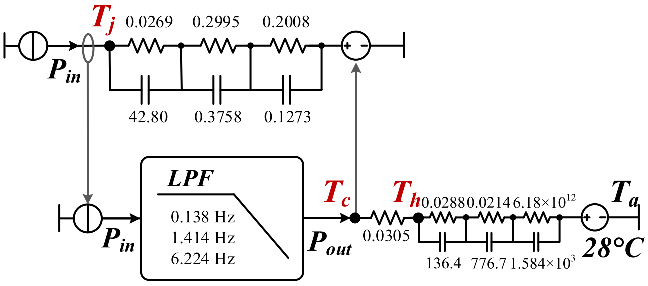

Fig. 15. Frequency-domain thermal model with parameters identified by proposed method.

critical frequencies of LPF are $f_1{}' = 0.138$, $f_2{}' = 1.414$, and $f_3{}' = 6.224$ Hz and the identified three-layer Foster thermal network is shown in Fig. 15. The ambient temperature T_a is set as constant 28 °C and a multilayer thermal impedance is used to offer accurate heatsink temperature.

The experimental and estimated thermal dynamics using the thermal model of Fig. 15 are shown in Fig. 16. As it can be seen, both estimated junction temperature and case temperature have a good agreement with experimental results after 0.05 s and the difference in junction temperature before 0.05 s is mainly caused by response time of sensors. In addition, another experiment under a step power-loss of 23.5 W has been conducted. The estimated and experimental temperatures are plotted in Fig. 17, which also shows that the temperature estimation agree with experimental results. It can be concluded that the proposed method is validated under different dissipated powers.

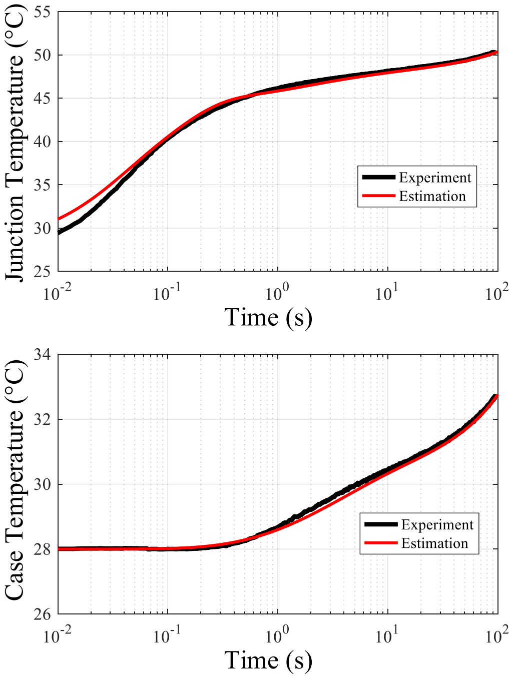

Fig. 16. Comparison of estimated temperatures of device under a step power-loss of 33.4 W into an IGBT module.

C. *Problems Caused by the Limitation of Measurement*

The limitation of the measurement is a key issue during experimental process because it determines the accuracy of extracted parameters. There are mainly two aspects: noise and bandwidth of the measurement.

The noise caused by the measurement directly influences the credibility of experimental results. As shown in Fig. 14(a), data of $P_{\mathrm{out}}(t)$ before 0.1 s are ignored due to the limitation of the accuracy of sensors. In this case, the following two solutions can be adopted: 1) by applying advanced measuring instrument with higher accuracy, and 2) by increasing the level of input power-loss P_{in}. The sensors applied in this article have a measurement range of -40 °C to $+250$ °C with an accuracy of ±0.3 to 0.8 °C. Since the sensors of case and heatsink are set very close to each other, the temperature difference between case and heatsink is relatively small under low level of input power-loss. In this case, the errors introduced by sensors become more significant. However, the errors can be reduced if advanced measuring instrument with higher accuracy and faster response time appear in the future. Moreover, if the input power-loss is

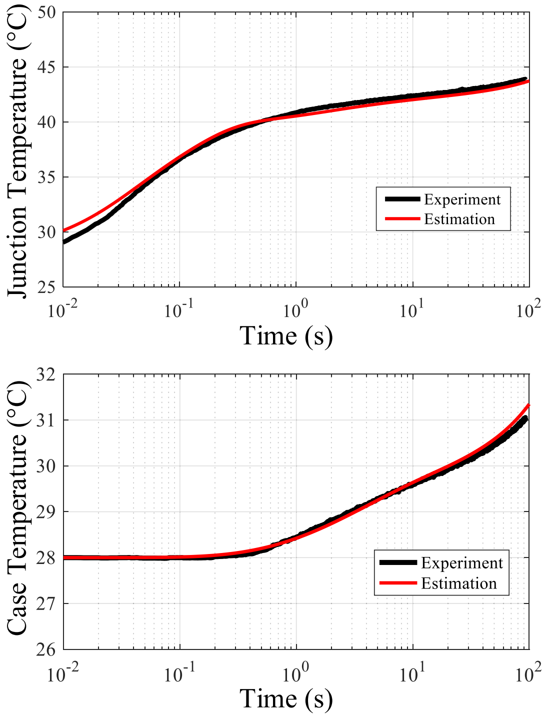

Fig. 17. Comparison of estimated temperatures of device under a step power-loss of 25.3 W into an IGBT module.

increased, the P_{out} curve will be smoother and the errors caused by the limitation of sensors will also be reduced.

The bandwidth is another important aspect of the measurement. Take the temperature sensors applied in this article as an example, the response time of sensors from datasheet is 5 ms, i.e., the recorded temperature data are invalid before 5 ms, corresponding to a cut-off frequency of 30 Hz. Then, the high-frequency behavior over 30 Hz will be filtered out. N is supposed as the actual number of critical frequencies of this power module. If there exists a critical frequency over 30 Hz in reality, the number of critical frequencies will be thereby reduced to $N-1$ limited by the measurement and the equation for P_{out} will be changed. In this case, the accuracy of highest frequency among the remaining $N-1$ critical frequencies will be influenced. Fortunately, the error of high-frequency band in LPF seems less important than low-frequency band, which has been proved in Fig. 7. It is expected that the significant estimation error for thermal behaviors will be experienced if the accuracy of low-frequency band of the second thermal path cannot be ensured. As a result, the number of critical frequencies in the equation for P_{out} may be less than the actual number if limited by the bandwidth of the measurement.

V. CONCLUSION

A new method to identify thermal parameters of the frequency-domain model for power semiconductor devices has been proposed in this article. Temperature responses of junction, case and heat sink under a step power-loss are measured simultaneously in order to obtain two critical curves, which contain information related to frequency-domain model. Then, mathematical fitting is applied to estimate thermal parameters of the model. The proposed method is validated by simulated and experimental results and is relatively simple compared with existing methods.

REFERENCES

[1] K. Ma, H. Wang, and F. Blaabjerg, “New approaches to reliability assessment: Using physics-of-failure for prediction and design in power electronics systems,” *IEEE Power Electron. Mag.*, vol. 3, no. 4, pp. 28–41, Dec. 2016.

[2] M. Ciappa, “Selected failure mechanisms of modern power modules,” *Microelectron. Rel.*, vol. 42, no. 4/5, pp. 653–667, 2002.

[3] C. Busca *et al.*, “An overview of the reliability prediction related aspects of high power IGBTs in wind power applications,” *Microelectron. Rel.*, vol. 51, no. 9–11, pp. 1903–1907, 2011.

[4] H. Wang *et al.*, “Transitioning to physics-of-failure as a reliability driver in power electronics,” *IEEE J. Emerg. Sel. Top. Power Electron.*, vol. 2, no. 1, pp. 97–114, Mar. 2014.

[5] V. Smet *et al.*, “Ageing and failure modes of IGBT modules in high-temperature power cycling,” *IEEE Trans. Ind. Electron.*, vol. 58, no. 10, pp. 4931–4941, Oct. 2011.

[6] U. M. Choi *et al.*, “Power cycling test and failure analysis of molded intelligent power IGBT Module under different temperature swing durations,” *Microelectron. Rel.*, vol. 64, pp. 403–408, 2016.

[7] M. Andresen, K. Ma, G. De Carne, G. Buticchi, F. Blaabjerg, and M. Liserre, “Thermal stress analysis of medium-voltage converters for smart transformers,” *IEEE Trans. Power Electron.*, vol. 32, no. 6, pp. 4753–4765, Jun. 2017.

[8] F. Hahn, S. Member, M. Andresen, and S. Member, “Thermal Analysis and balancing for modular multilevel converters in HVDC applications,” *IEEE Trans. Power Electron.*, vol. 33, no. 3, pp. 1985–1996, Mar. 2018.

[9] A. Isidoril, F. M. Rossi, F. Blaabjerg, and K. Ma, “Thermal loading and reliability of 10-MW multilevel wind power converter at different wind roughness classes,” *IEEE Trans. Ind. Appl.*, vol. 50, no. 1, pp. 484–494, Jan./Feb. 2014.

[10] R. Wu *et al.*, “A temperature-dependent thermal model of IGBT modules suitable for circuit-level simulations,” *IEEE Trans. Ind. Appl.*, vol. 52, no. 4, pp. 3306–3314, Jul./Aug. 2016.

[11] K. Ma, D. Zhou, and F. Blaabjerg, “Evaluation and design tools for the reliability of wind power converter system,” *J. Power Electron.*, vol. 15, no. 5, pp. 1149–1157, 2015.

[12] U. M. Choi, S. Jorgensen, and F. Blaabjerg, “Advanced accelerated power cycling test for reliability investigation of power device modules,” *IEEE Trans. Power Electron.*, vol. 31, no. 12, pp. 8371–8386, Dec. 2016.

[13] K. Ma, M. Liserre, F. Blaabjerg, and T. Kerekes, “Thermal loading and lifetime estimation for power device considering mission profiles in wind power converter,” *IEEE Trans. Power Electron.*, vol. 30, no. 2, pp. 590–602, Feb. 2015.

[14] S. H. Ali, M. Heydarzadeh, S. Dusmez, X. Li, A. S. Kamath, and B. Akin, “Lifetime estimation of discrete IGBT devices based on Gaussian process,” *IEEE Trans. Ind. Appl.*, vol. 54, no. 1, pp. 395–403, Jan./Feb. 2018.

[15] U. M. Choi, K. Ma, and F. Blaabjerg, “Validation of lifetime prediction of IGBT modules based on linear damage accumulation by means of superimposed power cycling tests,” *IEEE Trans. Ind. Electron.*, vol. 65, no. 4, pp. 3520–3529, Apr. 2018.

[16] H. Liu, K. Ma, Z. Qin, P. C. Loh, and F. Blaabjerg, “Lifetime estimation of MMC for offshore wind power HVDC application,” *IEEE J. Emerg. Sel. Topics Power Electron.*, vol. 4, no. 2, pp. 504–511, Jun. 2016.

[17] K. Ma, U. M. Choi, and F. Blaabjerg, “Prediction and validation of wear-out reliability metrics for power semiconductor devices with mission profiles in motor drive application,” *IEEE Trans. Power Electron.*, vol. 33, no. 11, pp. 9843–9853, Nov. 2018.

[18] I. Vernica, K. Ma, and F. Blaabjerg, “Reliability assessment platform for the power semiconductor devices—Study case on 3-phase grid-connected inverter application,” *Microelectron. Rel.*, vol. 76/77, pp. 31–37, 2017.

[19] U. M. Choi, F. Blaabjerg, S. Jorgensen, S. Munk-Nielsen, and B. Rannestad, “Reliability improvement of power converters by means of condition monitoring of IGBT modules,” *IEEE Trans. Power Electron.*, vol. 32, no. 10, pp. 7990–7997, Oct. 2017.

[20] S. Yang, D. Xiang, A. Bryant, P. Mawby, and S. Member, "Condition monitoring for device reliability in power electronic converters: A review," *IEEE Trans. Power Electron.*, vol. 25, no. 11, pp. 2734–2752, Nov. 2010.

[21] M. Andresen, K. Ma, G. Buticchi, J. Falck, F. Blaabjerg, and M. Liserre, "Junction temperature control for more reliable power electronics," *IEEE Trans. Power Electron.*, vol. 33, no. 1, pp. 765–776, Jan. 2018.

[22] D. A. Murdock, J. E. Ramos Torres, J. J. Connors, and R. D. Lorenz, "Active thermal control of power electronic modules," *IEEE Trans. Ind. Appl.*, vol. 42, no. 2, pp. 552–558, Mar./Apr. 2006.

[23] K. Ma, N. He, M. Liserre, and F. Blaabjerg, "Frequency-domain thermal modeling and characterization of power semiconductor devices," *IEEE Trans. Power Electron.*, vol. 31, no. 10, pp. 7183–7193, Oct. 2016.

[24] A. S. Bahman, K. Ma, and F. Blaabjerg, "A lumped thermal model including thermal coupling and thermal boundary conditions for high-power IGBT modules," *IEEE Trans. Power Electron.*, vol. 33, no. 3, pp. 2518–2530, Mar. 2018.

[25] H. R. Wickramasinghe, W. Wang, and G. Konstantinou, "Thermal performance of modular multilevel converters in HVDC applications under offset," in *Proc. 10th Int. Conf. Power Electron. ECCE Asia* , 2019, vol. 3, pp. 3–8.

[26] K. Ma and F. Blaabjerg, "Multi-timescale modelling for the loading behaviours of power electronics converter," in *Proc. IEEE Energy Convers. Congr. Expo.*, 2015, pp. 5749–5756.

[27] Y. Zhang, H. Wang, Z. Wang, and F. Blaabjerg, "Simplified multi-time scale thermal model considering thermal coupling in IGBT modules," in *Proc. Appl. Power Electron. Conf. Expo.*, 2019, pp. 319–324.

[28] R. Sander, M. Suriyah, and T. Leibfried, "Characterization of a countercurrent injection-based HVDC circuit breaker," *IEEE Trans. Power Electron.*, vol. 33, no. 4, pp. 2948–2956, Apr. 2018.

[29] V. De Nazareth Ferreira, A. F. Cupertino, H. A. Pereira, A. V. Rocha, S. I. Seleme, and B. De Jesus Cardoso Filho, "Design and selection of high reliability converters for mission critical industrial applications: A rolling mill case study," *IEEE Trans. Ind. Appl.*, vol. 54, no. 5, pp. 4938–4947, Sep./Oct. 2018.

[30] Y. Zhu, K. Ma, and X. Cai, "Thermal characterization method of power semiconductors based on H-bridge testing circuit," *IEEE Trans. Power Electron.*, vol. 34, no. 9, pp. 8268–8273, Sep. 2019.

[31] A. Hensler, D. Wingert, C. Herold, J. Lutz, and M. Thoben, "Thermal impedance spectroscopy of power modules," *Microelectron. Rel.*, vol. 51, no. 9–11, pp. 1679–1683, 2011.

[32] Z. Luo, H. Ahn, and M. A. El Nokali, "A thermal model for insulated gate bipolar transistor module," *IEEE Trans. Power Electron.*, vol. 19, no. 4, pp. 902–907, Jul. 2004.

[33] United States Department of Defense Test Method Standard: Microcircuits, Method 1012.1 Thermal Characteristics, Std. MIL-STD-883G, 1980.

[34] Thermal Test Chip Guideline (Wire Bond and Filp Chip). JEDEC Standard JESD51-4A, 2019.

Ke Ma (Senior Member, IEEE) received the B.Sc. and M.Sc. degrees in electrical engineering from Zhejiang University, Hangzhou, China, in 2007 and 2010, respectively, and the Ph.D. degree from Aalborg University, Aalborg, Denmark, in 2013. In 2014, he joined Aalborg University, as an Assistant Professor. He was a Part-Time Consultant with Vestas Wind Systems A/S, Denmark, in 2015. In 2016, he joined the Faculty of Shanghai Jiao Tong University, Shanghai, China, as a Tenure-Track Research Professor, and is presently the Deputy Director for the Key Laboratory of Control of Power Transmission and Conversion, Ministry of Education, China. His current research interests include power electronics and its reliability in the application of renewable energy, HVdc, and motor drive systems. Dr. Ma was the recipient of the "Thousand Talents Plan Program for Young Professionals" of China in 2016, the "Excellent Young Wind Doctor Award 2014" from the European Academy of Wind Energy, and several prize paper awards from IEEE. He is an Associate Editor for IEEE TRANSACTION ON INDUSTRY APPLICATIONS and IEEE JOURNAL OF EMERGING AND SELECTED TOPICS IN POWER ELECTRONICS.

Mengqi Xu (Student Member, IEEE) received the B.Sc. degree in electrical engineering from the Nanjing University of Aeronautics and Astronautics (NUAA), Nanjing, China, in 2018. She is currently working toward the Ph.D. degree in electrical engineering with Shanghai Jiao Tong University, Shanghai, China.

Her research interests include the thermal modeling and reliability analysis of power electronics.

Bo Liu received the B.Sc. degree from the Huazhong University of Science and Technology (HUST), Wuhan, China, in 2017, and the M.Sc. degree from Shanghai Jiao Tong University, Shanghai, China, in 2020, both in electrical engineering.

He is currently an Engineer with Huawei Technologies Co., Ltd, Shenzhen, China. His research focuses on the reliability of power electronic devices.